Supplementary Materials for

Climate variability off Africa's southern Cape over the past 260, 000 years

Karl Purcell *et al.*

Supplementary figures:
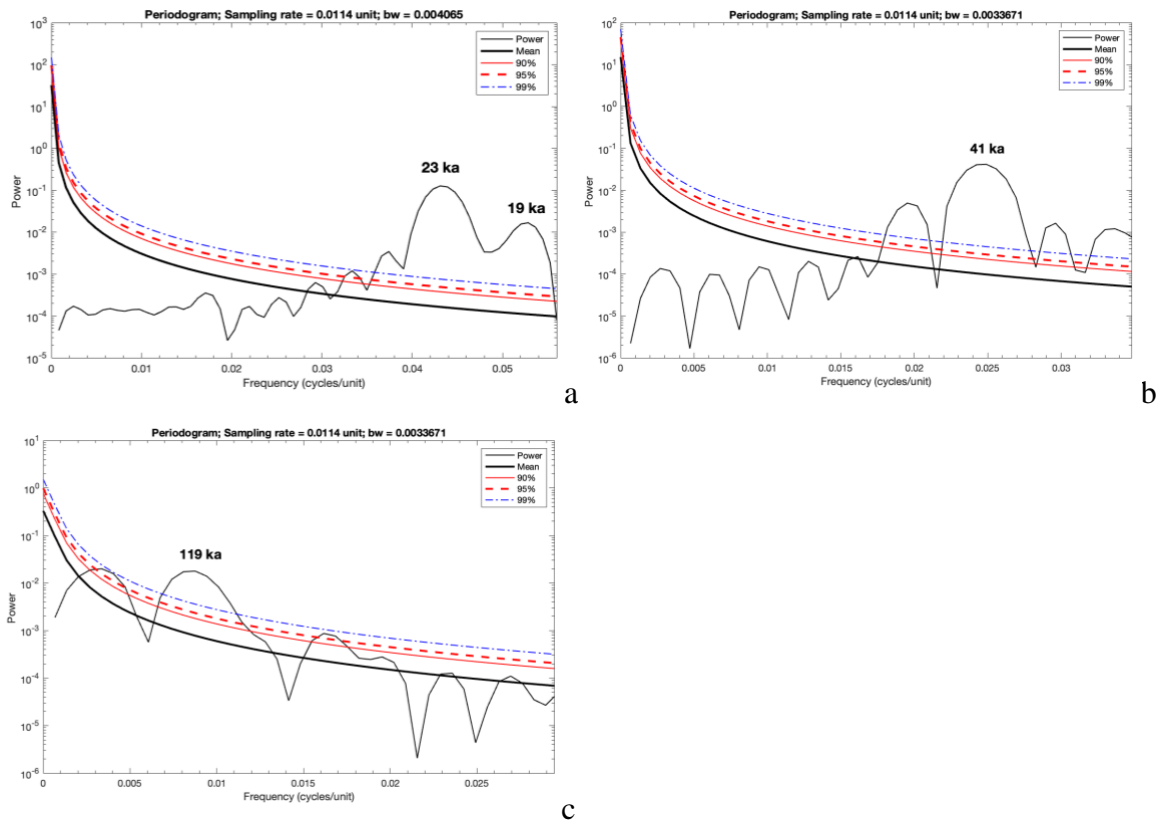
Fig. S1. a) Periodogram of precession index for 0-246 ka. Note the high power at 23 and 19 ka.
b) Periodogram of obliquity for 0-246 ka. Note the high power at 41 ka.
c) Periodogram of eccentricity for 0-246 ka. Note the high power at 119 ka.
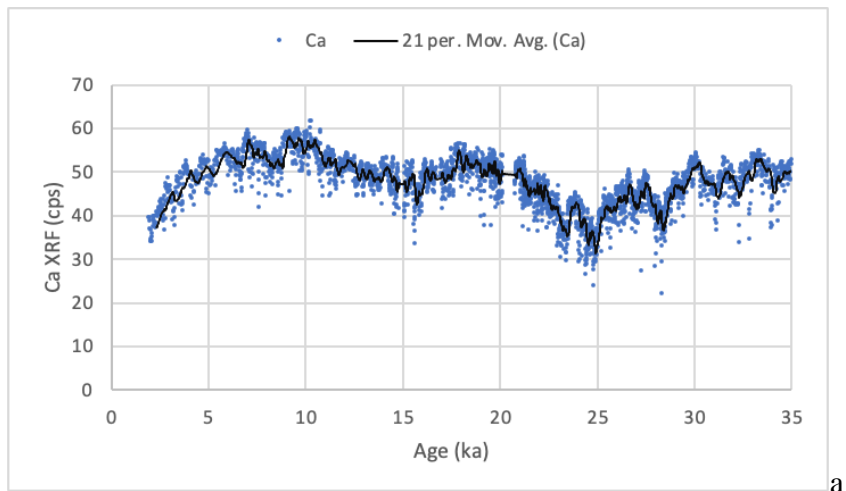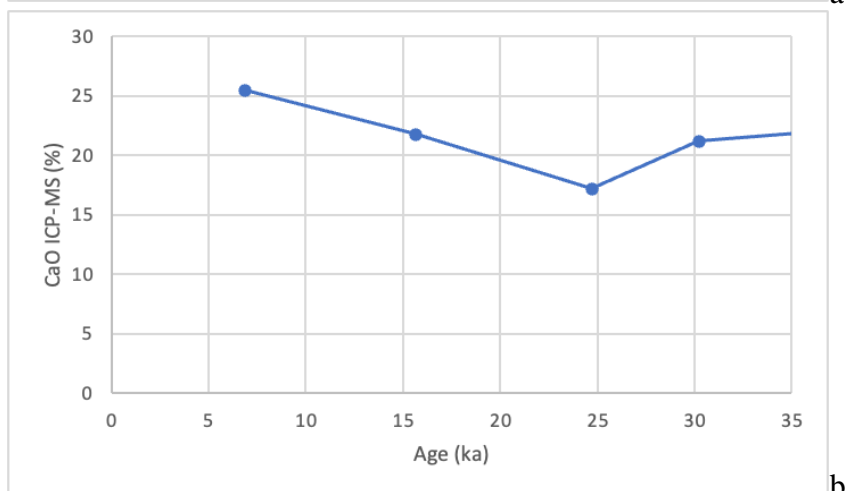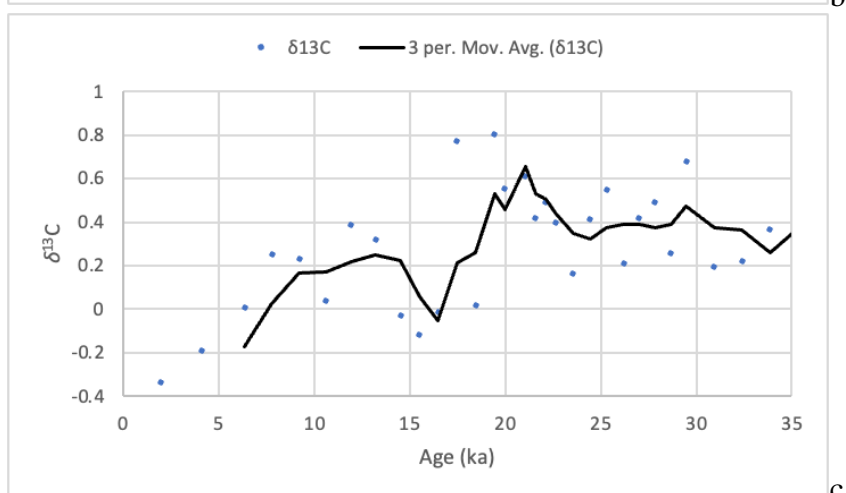
Fig. S2. a) Calcium XRF measurements for the last 35 ka. b) CaO ICP-MS measurements for the last 35 ka. c) $\delta^{13}C$ measurements on the G. ruber for the last 35 ka.
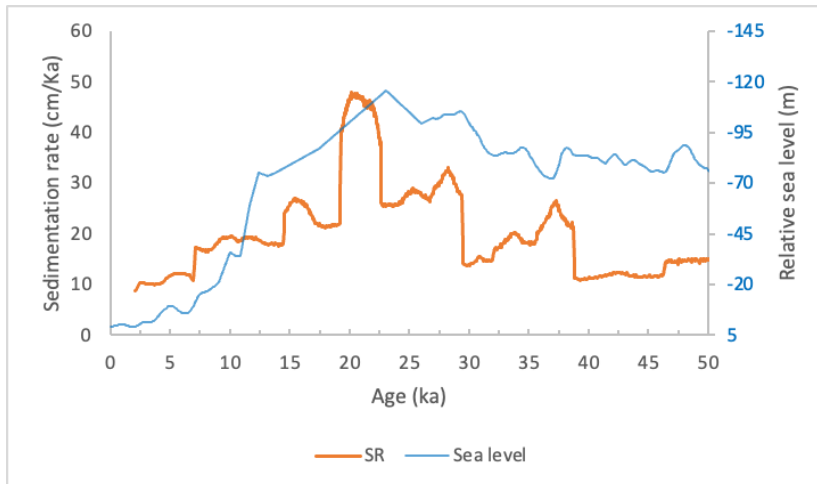
Fig. S3. Sedimentation rate of MD20-3592 vs relative sea level (Grant et a., 2012).

Figure S4: First core section, with indication of bioturbation around 22 cm depth (dark elliptic shape).
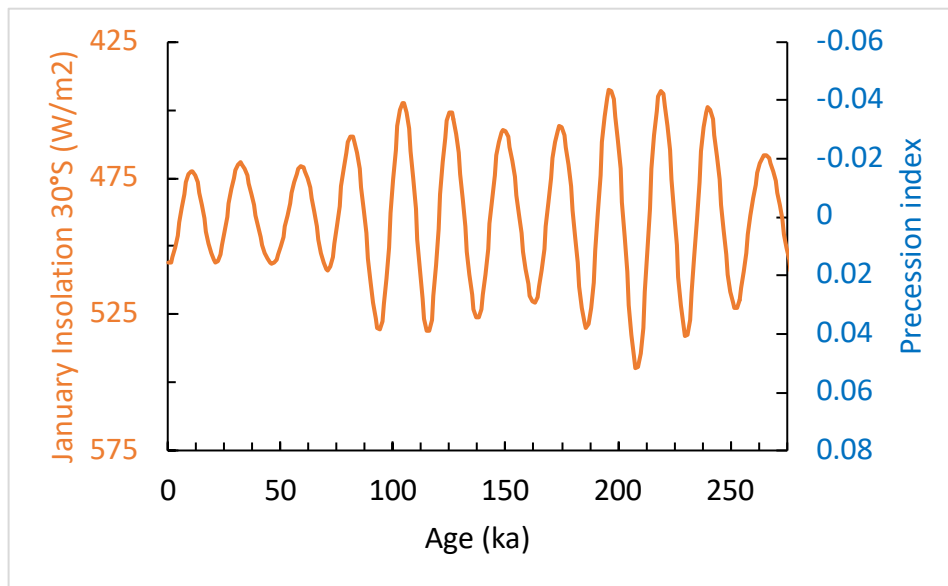
Figure S5. Local summer insolation vs Precession index.

X-ray fluorescence (XRF) core scanning

Before scanning the cores were warmed to room temperature, and the surface was smoothed and then covered with a thin transparent film to prevent drying of the sediments. The core sections were scanned with a molybdenum (Mo) tube operating at a voltage of 30 kV and a current of 40 mA[1] with a dwell duration of 10s. These parameters maximised the total number of counts per second during the analysis. The XRF spectra was then processed with the Q-Spec software (Croudace et al., 2006). Portions of the scanned data having spectral intensities below 2 sigma of Fe or K were removed, since they originated from air at the top and bottom of the core section, as well as with cracks and voids in the middle of the sections. Fe and K were chosen as they have strong intensities are used as indicators for terrestrial climate zones (Mulitza et al., 2008; Govin et al., 2012).

Calibration samples

Bergen XRF calibration samples method:
Around 0.1 g of freeze-dried and ground bulk sediment was ignited in a furnace at 1000 °C for loss-on-ignition (loi) to remove organic matter (Dean, 1974). The samples were then digested with a mixture of HNO_3 and HF in Savillex beakers on a heating plate at 135°C. The dissolved and dried samples were subsequently dissolved in 2N HNO_3. In cases where traces of undissolved oxides or sulfides were present, these were dissolved with small amounts of Aqua Regia (HNO_3/HCl 1:3). Before analysis, the samples were diluted in a solution of 2 % w/v HNO_3. Major elements (Al, B, Ba, Ca, Co, Cr, Cu, Fe, K, Li, Mg, Na Mn, Ni, P, Pb, S, Sr, Ti, V, Y, Zn, Zr) were measured using a Thermo Scientific ICap 7600 Inductively Coupled Plasma Atomic Emission Spectrometer (ICP-AES) at the University of Bergen. Trace elements (Ba, Co, Cr, Cs, Cu, Hf, Li, Mn, Nb, Ni, Pb, Rb, Sc, Sr, Ta, Th, Ti, U, V, Y, Zn, Zr, Ge, Mo and others) were measured with a Thermo Scientific Element XR High-Resolution Inductively Coupled Plasma Mass Spectrometer (HR-ICP-MS). For both major and trace elements, the international standard BCR2 was run along the sample's measurements. The relative standard deviation displayed a precision of 0.1 to 7.1% for the elements of interest in BCR2.

The results for the calibration samples produced at the University of Bergen can be found in table S1:

Depth interval	Al$_2$O$_3$	K$_2$O	TiO$_2$	Fe$_2$O$_3$	CaO
(cm)	(g/kg)	(g/kg)	(g/kg)	(g/kg)	(g/kg)
56-57	69.9	4.4	3.7	28.3	254.8
220-221	51.3	3.6	2.5	22.8	145.6
512-513	88.0	9.2	4.4	37.1	172.2
660-661	75.3	5.6	3.9	33.7	212.0
1120-1121	66.8	5.5	3.4	29.4	249.9
1320-1321	93.7	11.1	4.8	42.0	149.2
1504-1505	62.3	3.9	3.2	25.0	275.4
1628-1629	78.8	5.7	4.0	31.8	207.2
1836-1837	68.8	4.8	3.5	27.6	246.0
2100-2101	90.2	7.8	4.5	34.3	185.7
2212-2213	69.5	6.1	3.3	29.9	265.0
2400-2401	71.0	5.8	3.6	30.7	231.3
2832-2833	107.7	16.1	5.2	52.0	123.7
3000-3001	69.3	5.4	3.6	27.5	243.2
3200-3201	84.3	8.9	4.3	36.1	187.8
3390-3391	129.4	23.7	6.6	55.1	49.0
3480-3481	87.6	9.6	4.5	34.2	165.9
3700-3701	64.9	5.5	3.3	33.0	260.8
4002-4003	71.7	6.4	3.8	24.4	222.0
4166-4167	78.2	6.9	3.8	34.0	233.0

Table S2. Measured values in g/kg of selected element oxides for the calibration samples.

Calibration of XRF data

Elements of interest were divided by a common denominator element that was measured simultaneously (e.g., ln(K$_{XRF(cps)}$/Ca$_{XRF(cps)}$)). This ratio was also calculated for the ICP measured data (e.g., ln(K$_{ICP(wt\%)}$/ Ca$_{ICP(wt\%)}$)). Calcium was chosen as the common denominator because it had the strongest XRF average signal intensity and measured concentration. The log ratios of the XRF and ICP measurements then were linearly regressed against each other for elements of interest. The resulting equations could then be used to convert the XRF log-ratios to quantitative log-ratios and from then on to quantitative ratios *[E$^{(log-ratio)}$ = ratio]*.

Log calibration equation: y=ax + b, where x is the natural logarithm of the elemental ratios (ex: ln(Al(cps)/Ca(cps)). These equations are obtained from the linear trends of the log ratios of the reference measurements (y axis) plotted on the log ratios of the 1 cm integrated depth XRF intensities (x axis).

Ratio	a	b
Al/Ca	1.0789	6.3253
Si/Ca	0.9836	4.4825
K/Ca	1.5166	0.6854
Ti/Ca	0.8691	-0.9787
Fe/Ca	0.8759	-1.6546
Fe/K	0.3406	0.4547

Table S2. Calibration equation parameters a and b for the log calibration.

Spectral analysis

1) Power spectra: An autoregressive AR(1) red noise model was fitted to the spectrum to determine which peaks are significantly different from noise, with 90%, 95% and 99% confidence limits.
2) Gaussian filters: The data was first detrended, outliers were removed, and then it was resampled evenly. Then a Gaussian filter was applied, with the central value coming from the power spectra analysis and bandwidth of 5×10^{-6}.
3) Wavelet analysis: This type of analysis decomposes a time series into time-frequency space and allows to determine the dominant modes of variability and how they vary through time (Torrence and Compo, 1998). The colours indicate the power above red noise, while the black outline is the 95% confidence level. The colour scale is a base 2 logarithmic scale, and the colours indicate the squared correlation strength. The line shaped like a shield is the "cone of influence" and indicates where there are boundary effects.
4) Cross Wavelet Transform: The resulting figure is similar to the CWT figure, with the addition of arrows indicating the phase relationship. The Cross Wavelet Transform was performed on the gaussian filters of PC1 and their associated orbital signals with the function xwt in the Wavelet coherence MATLAB toolbox. This was done to determine whether the two time series share a high power at specific frequencies, and the nature of their phase relationship. A consistent phase relationship can be suggestive of causality between the time series (Grinsted et al., 2004).
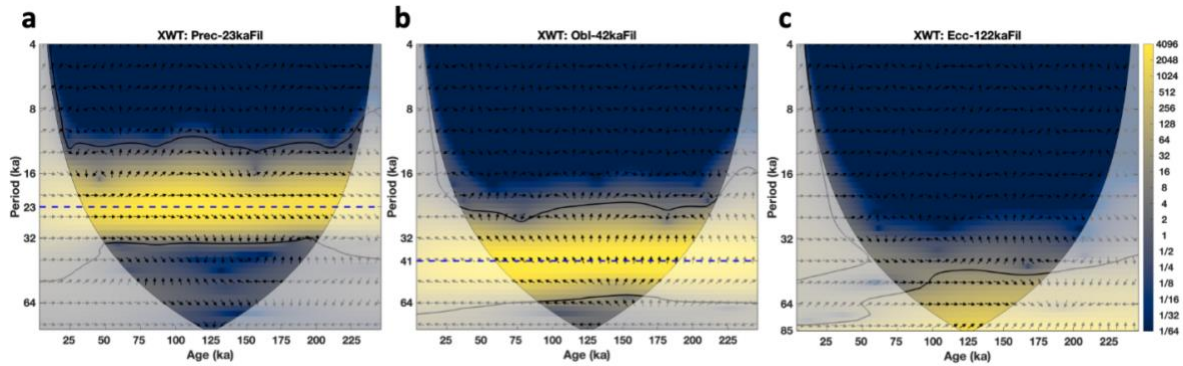
Figure S6. Cross Wavelet Transform. (**a**) Precession vs 23 ka filter. The colours indicate the wavelet power spectral density (PSD) in normalized units, using the cividis colour map. The black contour designates the 5% significance levels against red noise and the cone of influence (COI) is shown as a lighter shade. The black arrows indicate the relative phase of the covariance between the two time series in time-frequency space (Cappellotto et al., 2022). (**b**) Obliquity vs 42 ka filter. (**c**) Eccentricity vs 122 ka filter.

Figure S6 shows the cross wavelet transform of orbital parameters and the gaussian filters. In fig. 9 a), the orientations of the arrows from left to right in the contoured area indicate a linear, in phase relationship, while the arrows pointing slightly down from 250 ka to 100 ka indicate that the gaussian filter is slightly leading the orbital precession. In b), the arrows pointing up indicate that obliquity is leading the gaussian filter. After 125 ka, the arrows point more towards the left, indicating an anti-phase relationship. This interpretation should be taken cautiously, as a non-horizontal orientation can mean a complex non-linear covariation and out of phase situation. In c), a relationship between eccentricity and the 122 ka gaussian filter cannot be investigated with this method, as this frequency is outside the cone of influence. However, near the 100 ka periodicity, in the deepest part of the record the arrows point up which indicate that eccentricity is leading the gaussian filter.

Stable isotope measurements
Where duplicate measurements were made, an average of the measurement was made.

Orbital parameters
The orbital parameters were calculated with the following online calculator (Laskar et al., 2004):
http://vo.imcce.fr/insola/earth/online/earth/online/index.php
The precession illustrated is the longitude of the perihelion (Loutre, MF. 2009)

Reference

Dean, W.E., 1974. Determination of carbonate and organic matter in calcareous sediments and sedimentary rocks by loss on ignition; comparison with other methods. *Journal of Sedimentary Research*, *44*(1), pp.242-248.

Laskar, J., Robutel, P., Joutel, F., Gastineau, M., Correia, A.C. and Levrard, B., 2004. A long-term numerical solution for the insolation quantities of the Earth. *Astronomy & Astrophysics*, *428*(1), pp.261-285.

Loutre, MF. (2009). Precession, Climatic. In: Gornitz, V. (eds) Encyclopedia of Paleoclimatology and Ancient Environments. Encyclopedia of Earth Sciences Series. Springer, Dordrecht. https://doi.org/10.1007/978-1-4020-4411-3_194